OXFORD

International Journal of Neuropsychopharmacology, 2015, 1–16

doi:10.1093/ijnp/pyu090
Research Article

RESEARCH ARTICLE

The Morphological and Molecular Changes of Brain Cells Exposed to Direct Current Electric Field Stimulation

Simon J. Pelletier, MSc; Marie Lagacé, MSc; Isabelle St-Amour, PhD; Dany Arsenault, PhD; Giulia Cisbani, PhD; Audrey Chabrat, MSc; Shirley Fecteau, PhD; Martin Lévesque, PhD; Francesca Cicchetti, PhD

Centre de Recherche du CHU de Québec, Axe Neuroscience, Québec, QC, Canada (Mr Pelletier, Ms Lagacé, Drs St-Amour, Arsenault, Cisbani, and Cicchetti); Département de Psychiatrie et Neurosciences, Université Laval, Québec, QC, Canada (Drs Lévesque and Cicchetti); Centre de recherche de l'Institut Universitaire en Santé Mentale de Québec, Québec, QC, Canada (Ms Chabrat and Dr Lévesque); Laboratory of Canada Research Chair in Cognitive Neuroscience, Centre Interdisciplinaire de Recherche en Réadaptation et Intégration Sociale, Centre de Recherche de l'Institut Universitaire en Santé Mentale de Québec, Université Laval, Canada (Dr Fecteau); Berenson-Allen Center for Noninvasive Brain Stimulation, Beth Israel Deaconess Medical Center, Harvard Medical School, Cambridge, MA (Dr Fecteau).

Correspondence: Francesca Cicchetti, PhD, Centre de Recherche du CHU de Québec (CHUQ), Axe Neuroscience, T2-50, 2705 Boulevard Laurier, Québec, QC Canada, G1V 4G2 (francesca.cicchetti@crchul.ulaval.ca).

Abstract

Background: The application of low-intensity direct current electric fields has been experimentally used in the clinic to treat a number of brain disorders, predominantly using transcranial direct current stimulation approaches. However, the cellular and molecular changes induced by such treatment remain largely unknown.
Methods: Here, we tested various intensities of direct current electric fields (0, 25, 50, and 100V/m) in a well-controlled in vitro environment in order to investigate the responses of neurons, microglia, and astrocytes to this type of stimulation. This included morphological assessments of the cells, viability, as well as shape and fiber outgrowth relative to the orientation of the direct current electric field. We also undertook enzyme-linked immunosorbent assays and western immunoblotting to identify which molecular pathways were affected by direct current electric fields.
Results: In response to direct current electric field, neurons developed an elongated cell body shape with neurite outgrowth that was associated with a significant increase in growth associated protein-43. Fetal midbrain dopaminergic explants grown in a collagen gel matrix also showed a reorientation of their neurites towards the cathode. BV2 microglial cells adopted distinct morphological changes with an increase in cyclooxygenase-2 expression, but these were dependent on whether they had already been activated with lipopolysaccharide. Finally, astrocytes displayed elongated cell bodies with cellular filopodia that were oriented perpendicularly to the direct current electric field.
Conclusion: We show that cells of the central nervous system can respond to direct current electric fields both in terms of their morphological shape and molecular expression of certain proteins, and this in turn can help us to begin understand the mechanisms underlying the clinical benefits of direct current electric field.

Keywords: transcranial direct current stimulation, inflammation, GAP-43

Received: September 10, 2013; **Revised:** October 20, 2014; **Accepted:** October 25, 2014

Introduction

Transcranial direct current stimulation (tDCS) is a noninvasive therapy that uses a direct current electrical field (DCEF) to modulate neuronal activity (Nitsche et al., 2008; Bikson et al., 2009; Kabakov et al., 2012), which can have beneficial effects for months following its delivery (Benninger et al., 2010). There are 2 ways to deliver DCEF to the brain: via anodal or cathodal stimulation. Anodal tDCS usually induces an increase in cortical excitability, whereas cathodal tDCS provokes the opposite effect (Nitsche et al., 2008).

The method of tDCS has been trialed for a variety of neurological and psychiatric disorders, including major depression (Dell'osso et al., 2013), epilepsy (Auvichayapat et al., 2013), stroke (Joung Lee and Chun, 2013), and Parkinson's disease (Boggio et al., 2006; Benninger et al., 2010; Pereira et al., 2013). In addition, DCEF delivered via electrodes surgically placed into the spine has been safely used in patients with complete spinal lesions with significant motor and sensory improvements (Shapiro et al., 2005).

Recent animal studies, although still very few in number, have been instrumental in identifying a number of potential mechanisms by which tDCS could produce these beneficial clinical effects. In vivo studies in rodents have provided evidence that tDCS is not only neuromodulatory but can also exert neuroprotective effects as demonstrated in epilepsy and ischemia models (Kim et al., 2010; Kamida et al., 2011). More specifically, it has been shown that tDCS can increase growth cone development (Yoon et al., 2012; Auvichayapat et al., 2013), promote neurogenesis (Rueger et al., 2012), and modulate inflammatory responses (Jiang et al., 2012; Rueger et al., 2012; Peruzzotti-Jametti et al., 2013). Moreover, in animals with spinal cord injury, the therapy can induce axonal regeneration across scar tissues along with reducing scar tissue size (Borgens, 1999).

In addition to these encouraging results, tDCS offers several advantages over more invasive treatments such as deep brain stimulation (DBS), cell replacement, or gene therapies. First of all, tDCS has proven to be safe, well-tolerated and is inexpensive. Secondly, the size of the device and the simplicity of its mode of action make it easy for patients to use themselves. Nevertheless, although a promising therapy, the mechanisms of action are still unclear, so we set about looking at this with respect to the different cells of the central nervous system. This involved stimulating a range of cell lines in vitro, including N2a (neuronal-like cells), BV2 (microglia), and C8-D1A (astrocytes) cells as well as explants derived from the mouse ventral tegmental area (VTA) using a DCEF stimulation prototype that we developed specifically for these experiments. Here, we report on the viability and morphological and molecular changes seen in these different cells exposed to various DCEFs.

Materials and Methods

Electrotactic Chamber and DCEF Application

The design of the electrotactic chamber was based on previously described methodology (Song et al., 2007; Koppes et al., 2011) (Figure 1A-B). Polydimethylsiloxane (PDMS; Sylgard 184, Dow Corning, Midland, MI) was added to a microscope cover glass into a 100×20-mm tissue culture petri dish (Starstedt, Montreal, QC, Canada). The cover glass was removed and the PDMS cut to create a 50×24×0.2-mm chamber (an area of 12 cm^2 for cell seeding) that was placed in a new 100×20-mm tissue culture petri dish. Small reservoirs on each side of the chamber were delineated using a commercial silicone preparation (3140 MIL-A-46146 RTV Coating, Dow Corning) to help stabilize pH (Song et al., 2007) and to allow direct current flow exclusively within the chamber (Babona-Pilipos et al., 2012). Cells were seeded within the electrotactic chamber (Figure 1A-B). The reservoirs were connected to a central petri dish by agar bridges composed of glass tubes filled with sterile 1% agarose (J.T. Baker, Mansfield, MA) diluted in Dulbecco's Modified Eagle Medium (DMEM, Sigma-Aldrich, Oakville, ON, Canada). The side petri dishes housing the electrodes were also filled with sufficient volumes of DMEM and, if needed, additional media was added to ensure an adequate buffer zone. The electrodes were made of silver chloride (AgCl) wires (Pico Wire, Etobicoke, ON, Canada), of which the tip was stripped. They were connected to a current regulator, which was in turn connected to a direct current (DC) power supply delivering field strengths of 25, 50, or 100V/m (Figure 1C). This configuration allowed us to physically isolate the cells from pH variations and metallic wastes generated by the electrodes. The strength of the DCEF was measured at the extremities of the chamber using a multimeter recording device at 4, 8, and 24 hours of stimulation. Temperature (thermocouple device; Omega, Laval, QC, Canada) and pH (pH meter; Oakton, Vernon Hills, IL) of the culture medium for each cell type were closely monitored during a 24-hour stimulation period to ensure that observations collected were not due to changes in these parameters.

For explant cultures, tissues were stimulated with a slightly different methodology, using an approach in which the electrotactic chamber resembled that used by Cork et al. (1994). To create the electrotactic chamber, the explants, coated in a 3D matrix gel onto a 12-mm coverslip, were placed upside down between 1-mm–thick glass slides adjusted with a rotary tool (Dremel, Mississauga, ON, Canada). They were fixed with a commercial silicone preparation (3140 MIL-A-46146 RTV Coating, Dow Corning) 4 mm apart in the middle well of a 6-well plate (Starstedt) forming a 5 mm×4 mm×1 mm chamber (0.2 cm^2). The remaining procedure was as described for cell culture except that the reservoirs contained Neurobasal Medium (Invitrogen) instead of DMEM.

Cell Culture

Murine N2a neuroblastoma (ATCC, Burlington, ON, Canada), BV2 microglial (gift from Dr. Serge Rivest, CRCHUQ), and C8-D1A astrocytic cells (ATCC) were seeded at densities of 1.36×10^4 cells/cm^2 for N2a and BV2 cells and 3.64×10^4 cells/cm^2 for C8-D1A cells, taking into account cell division rates of each cell type. Cells were maintained in DMEM (D5796, Sigma-Aldrich) supplemented with 1× (100 units penicillin and 0.1 mg streptomycin/mL) (Sigma-Aldrich) as well as 10% fetal bovine serum (FBS, Sigma-Aldrich) for N2a and BV2 cells or 15% FBS for C8-D1A cells, all at 37°C and 5% CO_2. All cells underwent a 24-hour acclimatization period in the electrotactic chamber. N2a cells were first differentiated by serum starvation (0.5% FBS) for an additional 24 hours (Evangelopoulos et al., 2005) before the application of DCEFs. Some cultures of BV2 cells were exposed to 1 µg/mL of lipopolysaccharide (LPS) (Sigma-Aldrich) 24 hours prior to stimulation and their responses compared with non-LPS–activated cells. To control for potential migration of LPS in the electrical field (EF), the concentration of endotoxins was verified using the limulus amoebocyte lysate test (PYROGENT Plus Gel Clot LAL assay, Lonza Walkersville, Inc., Walkersville, MD) following the stimulation period. This confirmed the absence of leakage of LPS outside of the electrotactic chamber ($n=3$, $P>.05$ Kruskal-Wallis; data not shown). C8-D1A cells, which did not undergo

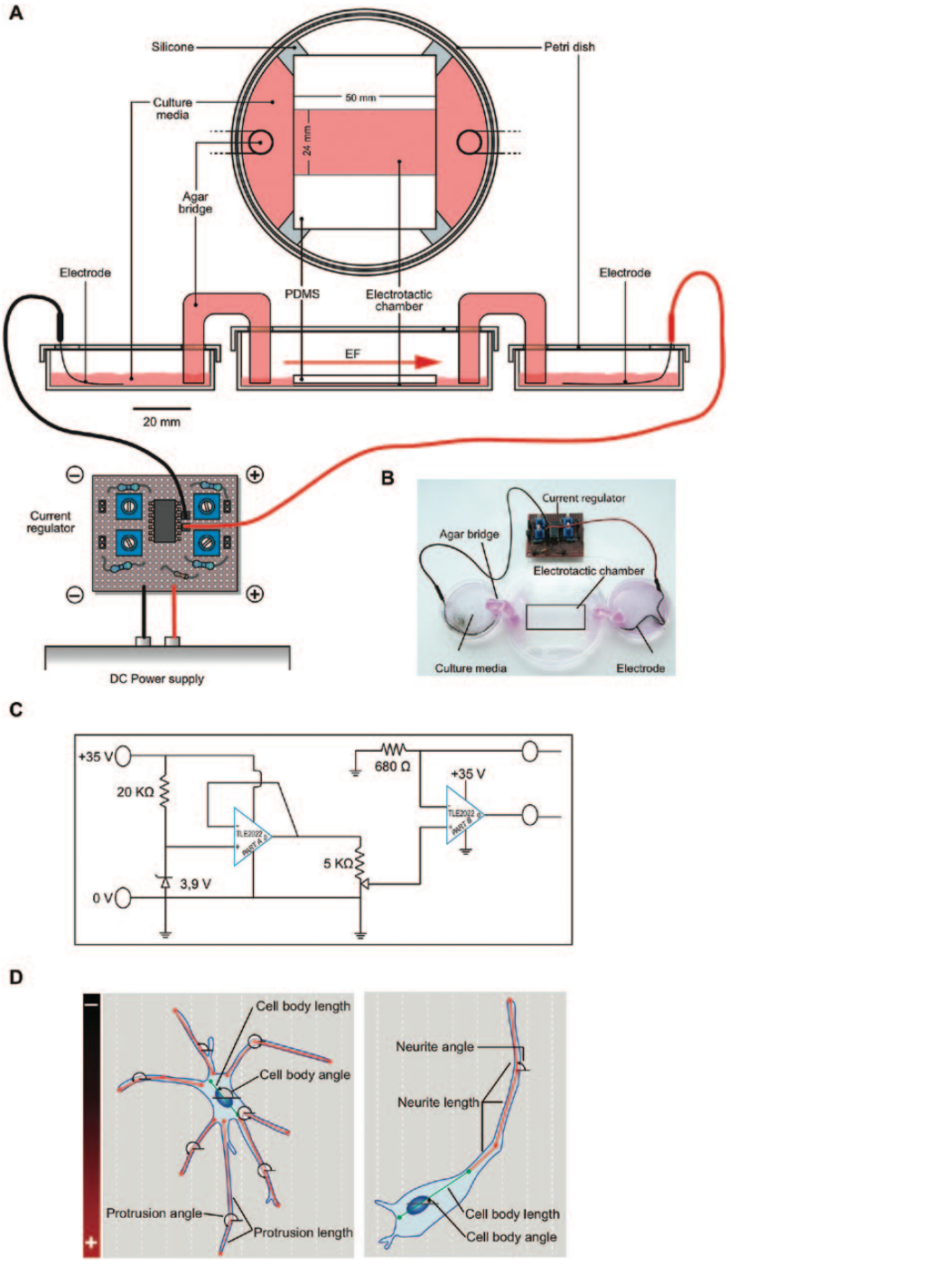

Figure 1. DCEF stimulation and quantification methodologies. (A-B) Schematic of the direct current stimulation prototype developed for in vitro experiments. A DC power supply is connected to a current regulator for allowing the application of exact voltages within the electrotactic chamber. The electrodes are placed in distinct petri dishes filled with culture media. These are in turn connected to a central petri dish - which houses the silicon chamber - by glass tubes loaded with agar gel, referred to as agar bridges. (C) Schematic of the current regulator. (D) Quantification methodology for protrusion, neurite, cell body length and angle orientation within the DCEF (astrocyte, left; neuron, right). DC, direct current; DCEF, direct current electrical field; EF, electric field; PDMS, polydimethylsiloxane; V, volt.

further manipulation, were immediately stimulated following the 24-hour acclimatization period. A Nikon Diaphot 300 Phase Contrast Inverted microscope (Mississauga, ON, Canada) with a QICAM digital camera using the QCapture software (QImaging, Surrey, BC, Canada) was used to acquire bright-field photomicrographs, which were used for the morphological analyses. A color filter detecting wavelengths >600 nm (Nikon, Ontario, Canada) was used to identify dead cells stained positively for propidium iodide (15 μM, Invitrogen, Burlington, ON, Canada).

Protein Extraction from Cell Cultures and Western Immunoblotting

Cells were lysed by 5×1 second sonication on ice in lysis buffer (50mM Tris 150mM sodium chloride (NaCl), 1.0% Triton X-100, 0.5% sodium deoxycholate, and 0.5% sodium dodecyl sulfate (SDS), pH 7.4, all from Sigma-Aldrich) supplemented with a complete protease inhibitor cocktail (Roche, Laval, QC, Canada), 10mg/mL pepstatin A, and the phosphatase inhibitor cocktail 2 (Sigma-Aldrich).

Samples were then centrifuged at 13200rpm at 4°C for 5 minutes and the supernatant was collected. The protein concentration of each sample was determined using a bicinchoninic acid (BCA) protein assay kit (Pierce, Rockford, IL) according to the manufacturer's protocol. Proteins (10 µg per well) were separated on 8% polyacrylamide SDS-polyacrylamide gel electrophoresis (SDS-PAGE) and transferred onto polyvinylidene fluoride membranes (EMD Millipore). Nonspecific binding was blocked with 5% nonfat dry milk and 0.5% bovine serum albumin (BSA) in phosphate buffered saline (PBS)-0.05% Tween 20 for 1 hour. Membranes were probed with the following primary antibodies: cyclooxygenase-2 (COX-2; Cayman Chemical, Ann Arbor, MI), glyceraldehyde-3-phosphate dehydrogenase (GAPDH; Abm, Richmond, BC, Canada), glial derived neurotrophic factor (GDNF; BioVision, Milpitas, CA), growth associated protein-43 (GAP-43; Novus Biological, Littleton, NH), and inducible nitric oxide synthase (iNOS; Sigma-Aldrich), all at dilutions of 1:1000. Blots were incubated with horseradish peroxidase (HRP)-conjugated anti-mouse and anti-rabbit secondary immunoglobulin G antibodies (Jackson ImmunoResearch, West Grove, PA) and visualized by chemiluminescent reagents (Luminata Forte, EMD Millipore). The optical density of each band was quantified using a KODAK Image Station 4000 MM Digital Imaging System and the Molecular Imaging Software (Carestream Health, Rochester, NY).

Cytokine and Chemokine Quantification in the BV2 Culture Media

Following the 24-hour stimulation episode, the culture media of BV2 microglial cells was collected. Floating cells were spun at 1500 rpm and the supernatant was collected and stored at –80°C. Cytokine and chemokine concentrations were quantified using an enzyme-linked immunosorbant assay (ELISA)-based chemiluminescent assay, the Q-Plex Mouse cytokine – Screen (16-Plex) (Quansys Biosciences, Logan, UT) following the manufacturer's protocol. The plate was read with a myECL Imager (Thermo Scientific, Whaltam, MA). The concentration of each cytokine was quantified with the Q-View Software (Quansys Biosciences). The following cytokines were detected: interleukin (IL)-1α, IL-1β, IL-2, IL-3, IL-4, IL-5, IL-6, IL-10, IL-12p70, IL-17, monocyte chemoattractant protein-1 (MCP-1), interferon gamma (IFN-γ), tumor-necrosis factor alpha (TNFα), macrophage inflammatory proteins (MIP), granulocyte-macrophage colony-stimulating factor (GM-CSF), and regulated on activated, normal T cell expressed and secreted (RANTES).

Animals

Male *Pitx3-green fluorescent protein* (*GFP*) transgenic mice were housed in our breeding facility and kept in ventilated cages under standard laboratory conditions. These mice express the *eGFP* reporter under the control of *Pitx3*. The expression of GFP colocalizes with tyrosine hydroxylase (TH), the enzyme responsible for the ultimate conversion of dopamine, allowing the visualization of dopaminergic neurons in the substantia nigra and VTA (Zhao et al., 2004b). Mice were mated with CD-1 females overnight, and the presence of a vaginal plug marked gestational day 0.5. Embryos were isolated from pregnant mice at embryonic day 14.5 (E14.5) and the VTA dissected. All animal experiments were performed in accordance with the Canadian Guide for the Care and Use of Laboratory Animals, and all procedures were approved by the Institutional Animal Care Committee of Laval University.

Explant Culture

The VTA of E14.5 *Pitx3*-GFP heterozygous embryos was isolated in chilled L-15 media (Invitrogen) and dissected into small explants of 450- to 500-µm segments. The explants were cultured in 24-well tissue culture plates (Sarstedt, Montreal, QC, Canada) on 12-mm–diameter coverslips coated with Matrigel (BD Bioscience, Mississauga, ON, Canada). A droplet of Matrigel (approximately 10 µL) was placed over it to form a 3D environment favorable to neurite growth. After gel polymerization, 800 µL of Neurobasal Medium (Invitrogen) with 2% B-27 Serum-Free Supplement (Invitrogen), 1% sodium pyruvate (Invitrogen), 1% L-glutamine (Invitrogen), 1× penicillin and streptomycin (Sigma-Aldrich), and 10% heat-inactivated FBS (Sigma-Aldrich) was added to each well. The explants were incubated at 37°C and 5% CO_2 for 72 hours. After incubation, cultured explants were transferred to the electrotactic chambers for 24 hours of stimulation. Explants were then fixed in 2% paraformaldehyde (J.T. Barker) in PBS, pH 7.4 (Sigma-Aldrich), for 30 minutes, prior to immunofluorescence staining.

Immunofluorescence Staining

Following a 24-hour stimulation session, the PDMS mold forming the electrotactic chamber was removed. N2a, BV2, and C8-D1A cells were fixed for 15 minutes in the petri dish with 4% paraformaldehyde and permeabilized with 0.1% Triton X-100 (Sigma-Aldrich) for phalloidin immunofluorescent staining. Cells or explants were then blocked in 1% BSA (EMD Millipore, Gibbstown, NJ) and stained with 100 units of phalloidin (Invitrogen) for 30 minutes, followed by µg/mL 4',6-diamidino-2-phenylindole (DAPI; Invitrogen). For the microscopic studies, a 60×22-mm coverslip was mounted over the cell area with Fluoromount Aqueous Mounting Medium (Sigma-Aldrich), and the bottom of the dish was cut with a rotary tool (Dremel). The explants were blocked and permeabilized with 10% normal goat serum (Sigma-Aldrich) and 0.1% Triton X-100 in 0.1M PBS for 1 hour at room temperature. They were subsequently incubated overnight at 4°C with a rabbit anti-TH primary antibody (Pelfreez, Rogers, AR) (1:1000) followed by AlexaFluor-488 conjugated goat anti-rabbit immunoglobulin G (Invitrogen) (1:100) at room temperature for 2 hours. The explants were photographed at 10× magnification using a LSM Pascal confocal microscope (Carl Zeiss Canada Ltd, Toronto, ON, Canada).

Morphological Analyses of Neuronal, Glial Cell Lines, and VTA Explant Cultures

Cellular protrusions from BV2 and C8-D1A cells and neurites from N2a-differentiated neurons as well as orientation of the cell bodies and protrusions were quantified using the Fiji image analysis software (NIH plugin NeuronJ, NIH, Bethesda, MD), as illustrated in Figure 1D. To quantify the effects of the DCEF on protrusion orientation, explants were photographed and acquired images divided into 4 equal quadrants: a quadrant for the cathode, one for the anode, as well as 2 lateral quadrants (Gil and del Rio, 2012). The length of all neurites was measured on each explant (Fiji image software) for each condition (0 and 50V/m). The total number and length of TH+ neurites within the cathodal and anodal quadrants were also analyzed.

Statistical Analyses and Image Preparation

All statistical analyses were performed in collaboration with M. Gaétan Daigle from the Service de Consultation Statistique of Université Laval using the SAS software (SAS Institute Inc., Cary, NC), JMP 11.0.0 (SAS Institute Inc.), and Prism 6.0 (GraphPad Software, LaJolla, CA). The graphs were prepared using Prism 6.0 (GraphPad) except for the circular scatterplots, for which we used the Oriana software (Kovach Computing Services, Isle of

Anglesey, Wales, UK). All images were prepared for illustration using Adobe Photoshop CS5 and Adobe Illustrator CS5.

Results

DCEF Effects on Viability, Morphology, and Cell Responses

To analyze the effects of DCEFs on neuronal-like cells, differentiated N2a cells were exposed to 0, 25, 50, and 100V/m DC stimulation for 24 hours (Figure 2). None of these experimental conditions (25, 50, 100V/m) induced significant cell death as revealed by propidium iodide staining (Figure 2A), nor did the various DCEFs affect the percentage of neuronal cells with neurite outgrowth which was used as a sign of cell differentiation (Evangelopoulos et al., 2005) (Figure 2B). However, the neurites were longer in all experimental conditions and this correlated with DCEF intensity (Figure 2D, H-K; Table 1). In addition, DCEF influenced the orientation of the neurites towards the cathode (Figure 2E, H-K); the greater the intensity of the EF applied, the more the neurites aligned in the direction of the cathode. Corroborating these morphological changes, the application of 25 or 50V/m DCEF increased cellular levels of GAP-43 (Figure 2C), a protein largely expressed in growth cones (Biewenga et al., 1996).

In addition to altering neurite properties, DCEFs had a direct effect on the cell body of differentiated N2a cells. The length of the cell body was significantly increased with 25 and 50V/m stimulation but not at 100V/m or in the absence of stimulation (Figure 2F). Cell bodies also responded to DCEFs by changing their orientation such that they aligned themselves parallel to the EF (Figure 2G, scatterplots).

DCEF Effects on Dopaminergic Explants

To test the effects of DCEFs on specific cell populations such as dopaminergic neurons, we used VTA explants derived from embryos of *Pitx3-GFP* mice. After a 24-hour stimulation with 50V/m DCEF, virtually all TH+ neurites grew towards the cathode (Figure 3A-C). However, the 50V/m DCEF did not change the number of neurites (data not shown), which was significantly lower in the direction of the anode compared with the cathode (Figure 3D).

DCEF Effects on Viability, Morphology, and Microglial Cell Responses

We next assessed the impact of 0 to 100V/m DCEF on microglial cells using the BV2 murine cell line. To reproduce the hallmark of a cerebral inflammatory response, BV2 cells were analyzed both in a resting and LPS-activated state (Figure 4). Although the viability of resting microglial cells was slightly different between DCEFs conditions, it was not significantly different from the control condition (Figure 4A). Cells demonstrated better viability following exposure to 50V/m than to 25 and 100V/m DCEFs. However, the viability of LPS-activated BV2 cells significantly decreased with increasing intensity of the DCEFs (Table 1).

When quiescent BV2 cells were stimulated, a higher percentage of cells with protrusions was observed at 25 and 50V/m compared with the control and 100V/m condition (Figure 4B, G-J), an effect that followed a second-order polynomial regression, meaning that cells show a peak response at 50V/m but with similar reactions at 0 and 100V/m (Table 1). A similar pattern was observed for the length of the protrusions (Figure 4C, G-J). However, when LPS-activated microglial cells were stimulated, the percentage of BV2 cells with protrusions, as well as the length of these protrusions, was significantly reduced in all experimental conditions when compared with control. These reductions negatively correlated with DCEF intensity (Figure 4B-C, K-N; Table 1). The length of the protrusions was significantly higher in LPS-activated compared with quiescent cells under 0, 25, and 100V/m stimulation (Figure 4C). The pattern of protrusion orientation in LPS-activated cells revealed an even distribution of protrusions in the DCEF with no preferred direction of growth. However, at a 100V/m stimulation of resting cells, there was a reorientation of the protrusions so that they were parallel to the DCEF (Figure 4D). Although changes in cell body length were not observed in quiescent cells, there was a reduction in cell body length in LPS-activated cells in all experimental conditions compared with control, with the most striking effect at 100V/m (Figure 4E). In control conditions (0V/m), the length of the cell body was significantly increased in LPS-activated compared with quiescent BV2 cells. Only in resting conditions were cell bodies depicting a significant orientation shift, which was parallel to the EF and was also seen with 50V/m and 100V/m DCEFs (Figure 4F).

To further study the impact of DCEFs on microglial cells, we quantified cytokine secretion and expression levels of COX-2 (Alhouayek and Muccioli, 2014) and iNOS (Vejlstrup et al., 1998) (Figure 5). Using ELISA assays, we found that cytokine levels secreted in culture media were similar in all conditions (Table 2) and that the concentration of iNOS was not modified by DCEF (Figure 5B). However, in resting BV2 cells, a 100V/m stimulation induced a significant increase in COX-2 protein levels (Figure 5A).

DCEF Effects on Viability, Morphology, and Astrocyte Responses

The cell viability (Figure 6A) and percentage of astrocytes developing protrusions (Figure 6B) were similar in all experimental conditions. C8-D1A cells were characterized by elongated protrusions in all experimental conditions when compared with the control setting (Figure 6C, G-J). The orientation of the protrusions was uniform for all conditions except at 100V/m, where they were reoriented perpendicularly to the DCEF (Figure 6D). The cell body length was increased with DCEF intensity and followed a linear regression (Figure 6E, G-J; Table 1). Cell bodies also oriented themselves, so that they were perpendicular to the DCEF, with an increasing number pointing in the same direction with increasing DCEF intensity (Figure 6F). Despite the morphological changes observed in astrocytes, we failed to detect significant changes in glial derived neurotrophic factor protein levels (n=2; data not shown).

Discussion

Weak extracellular DCEFs can alter the migration, shape the morphology, and influence the growth and metabolism of a number of cell types (for review; Pelletier and Cicchetti, 2014 and see Table 3). In this study, we built on these observations and now further report on the viability, morphological phenotypes, and various responses in the major cell types of the central nervous system: neurons and glial cells (Table 4).

For this particular study, we chose to work with immortalized cell lines because of their homogeneity and reproducibility in vitro. We thus selected 3 commonly used cell lines. The N2a cells (N2a murine neuroblastoma cells) have been widely used to study a variety of cellular processes (Jacobsson and Fowler, 2001;

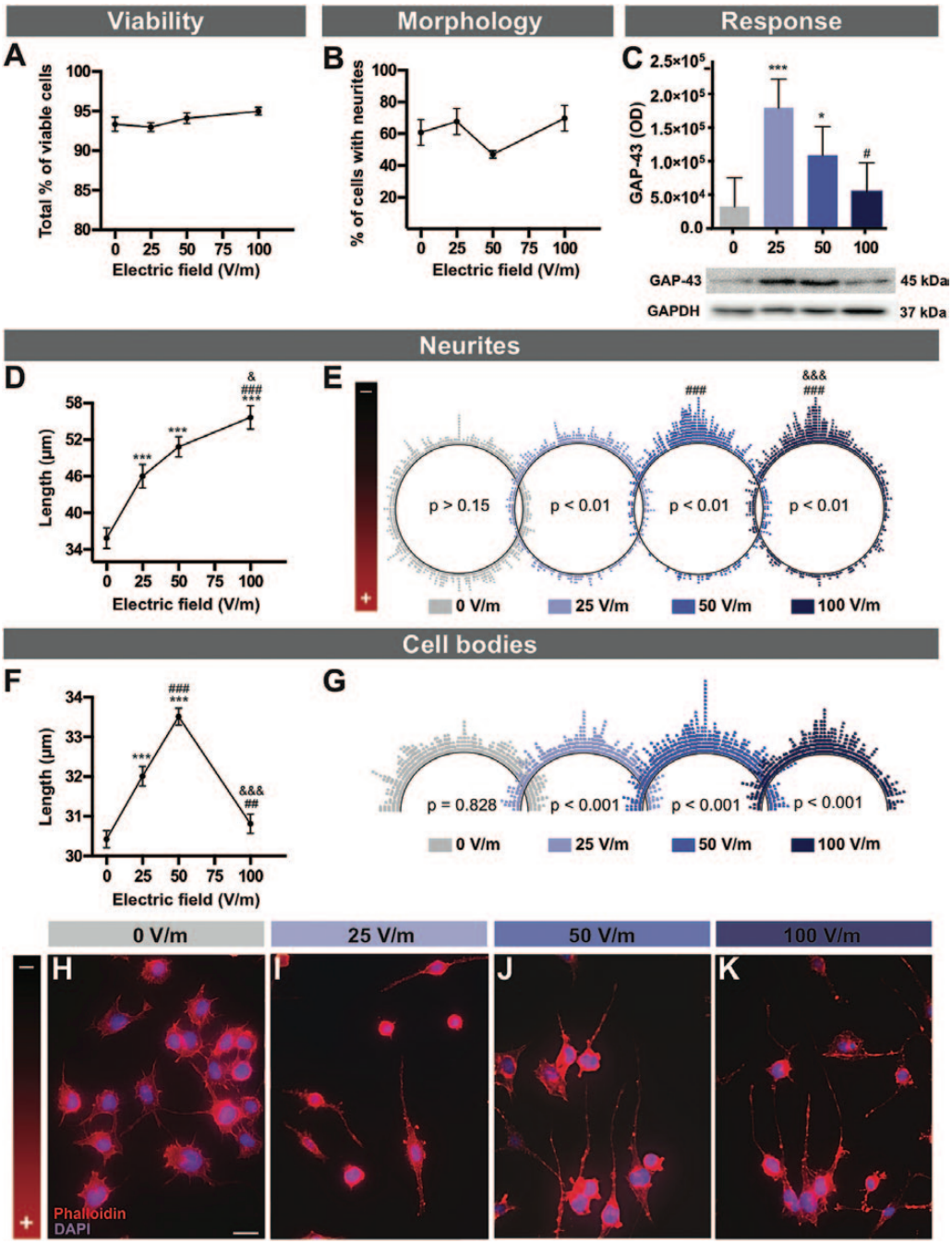

Figure 2. DCEF effects on neuronal elements. N2a mouse cells were differentiated into neuronal-like cells and various aspects relating to viability (A), morphology (B), and response (C) were assessed following exposure to increasing DCEFs (0, 25, 50, and 100V/m). (A) The total percentage of viable N2a cells (as measured in 3–4 replicates, n total = 877–1900 cells) as well as the percentage of viable N2a cells specifically depicting neurites (5–6 replicates, n total = 901–1134) was similar across all DCEFs applied (from 0 to 100V/m). (C) Protein concentration for GAP-43, a molecule expressed during axonal/neurite growth, was increased following a 24-hour stimulation of 25 and 50V/m (graph depicting average data of 4 replicates). (D) Measurements of total neurite length revealed significant elongation (5–6 replicates, n total = 449–624) (E) as well as a shift of orientation towards the cathode (5–6 replicates, n total = 449–624) when cells were stimulated at 25, 50, and 100V/m. The polar distribution of neurite angles (each dot represents the angle of a single neurite) demonstrates a significantly more prominent orientation towards the cathode at 50 and 100V/m. (F) Additionally, the 25 and 50 V/m DCEFs had a significant effect on the total length of the cell body (5–6 replicates, n total = 493–688) when compared with cells exposed to 0 or 100V/m DCEF. (G) Polar distribution of cell body angles (each dot represents the angle of a single cell body) reveals that cell angles reorient parallel to the DCEF. (H-K) Photomicrographs of double phalloidin (F-actin, red) and DAPI (nucleus, blue) immunofluorescent staining illustrating the morphological and orientational changes in N2a cells in response to DCEFs (scale bar: 20 µm). (A-D, F) The values represent LS-means ± SEM. Statistical analyses were performed using ANOVA (split-plot-type) (A-D, F). (E) Kuiper's Test of Uniformity and (G) chi-square test using grouped data (number of classes = 8 with identical divisions for interval 0–180°). $^{***}P < .001$ vs 0V/m; $^{\#\#}P < .01$, $^{\#\#\#}P < .001$ vs 25V/m; $^{\&}P < .05$, $^{\&\&\&}P < .001$ vs 50V/m. DCEF, direct current electrical field; GAP-43, growth associated protein-43; GAPDH, glyceraldehyde 3-phosphate dehydrogenase; LS, least square; OD, optical density; V/m, Volt/meter.

Alais et al., 2008; Wang et al., 2011). BV2 cells are used in vitro as a model of microglia, because they have been shown to respond to pharmacological agents and demonstrate normal microglial function, such as phagocytosis. Compared with primary microglia, the BV2 cells have similar cell activation patterns to LPS stimulation, including the activation of inflammation-related

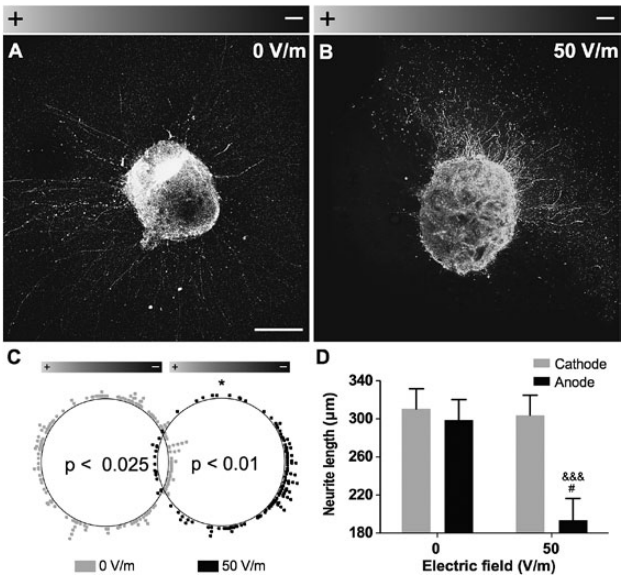

Figure 3. DCEF effects on dopaminergic explants. (A-B) Photomicrographs of VTA explants obtained from E14.5 *Pitx3*-GFP transgenic mice in control condition (0V/m) or following a 24-hour exposure to a 50-V/m DCEF (n = 3 explants per condition). Scale bar: 200 µm. (C) Polar scatterplot depicting the orientation of neurite outgrowth for each condition, where each dot represents the end point of a single neurite. A significant orientation shift towards the cathode was observed in the 50-V/m condition. (D) The total neurite length, as measured within the delineated quadrants corresponding to the anode and the cathode, was also significantly decreased following a 50-V/m DCEF application. Values are expressed as LS-means ± SEM. Statistical analyses were performed using the (C) Kuiper's Test of Uniformity, (D) the Mann-Whitney following log transformation. $^{*}P < .05$ vs 0V/m; $^{\#}P < .05$ vs anode, 0V/m; $^{\&\&\&}P < .0001$ vs Cathode, 50V/m. DCEF, direct current electrical field; LS, least square; V/m, Volt/meter.

kinases (JNK and p-38) and transcription factors (nuclear factor kappa-light-chain-enhancer of activated B cells (NF-kB) and c-Jun) as well as the release of inflammatory mediators (eg, TNFα, IL-1β, and nitroc oxide (NO)) (Henn et al., 2009). Finally, we used the type-1 astrocyte cell line (C8-D1A cells, ATCC), which expresses GFAP and displays the classic morphology of these cells (Booth and Kim, 2012).

We first demonstrated that the viability and number of N2a murine cells differentiated into neurons were not affected by DCEFs. The cells responded to DCEFs, as shown by their neurite outgrowth and their alignment in the EF. Although this neurite outgrowth effect of DCEF in N2a cells has been observed (Jain et al., 2013), there have been no previous reports on their alignment in the EF (Table 3). The elongation of neuronal processes towards the cathode is a phenomenon, however, now widely recognized. It is hypothesized to be caused by changes in the gating of Ca^{2+} at the growth cone of the neurite and by the electrophoretic or electroosmostic movements of membrane receptors (Borgens et al., 1994; McCaig et al., 2005). The reorganization of the cytoskeleton has also been suggested to play a role (Zhao et al., 2004).

Supplementing these observations, we described that cell bodies repositioned their orientation in the EFs. We also found an increase in GAP-43 levels, a protein expressed in neuronal growth cones during synaptogenesis and axonal development/regeneration (Biewenga et al., 1996), although neurite length, which corresponds to overall growth, and the expression of GAP-43 did not follow a linear pattern. In other words, GAP-43 expression did not augment with neurite length at 50-V/m stimulation or higher. Despite the fact that GAP-43 has been reported to correlate with axonal/neurite elongation (Meiri et al., 1986; Biffo et al., 1990; Benowitz and Routtenberg, 1997), it has also been described to be absent in dendrites of hippocampal neurons in culture (Goslin et al., 1988) and is not necessary for PC12 neurite outgrowth (Baetge and Hammang, 1991). Alternatively, GAP-43 has been associated with axonal sprouting (Aigner et al., 1995; Buffo et al., 1997), which indicates a potential involvement in neurite sprouting rather than elongation. Taken together, our results nevertheless support the increase in GAP-43 levels previously measured after anodal tDCS in ischemic rodent brains (Yoon et al., 2012). To further explore the effects of DCEF on neuronal populations, we applied DCEF to VTA explants from *Pitx-3-GFP* mice, allowing the visualization of dopaminergic neurons, a cell population that would be of particular interest in the treatment of Parkinson's disease with tDCS. With a stimulation of 50V/m, we observed that the dopaminergic neurites reoriented towards the negative pole of the EF, the cathode.

We next examined the impact of DCEFs on microglia. BV2 microglial cells can rapidly change their morphology in response to environmental cues, showing a highly ramified phenotype (Sheng et al., 2011) and transiting from an inactivated amoeboid to an elongated shape (Michaud et al., 2013). The activation of microglial cells also induces a dramatic change in protein expression (eg, proinflammatory cytokines). The expression of COX-2 and iNOS, respectively responsible for the synthesis of prostaglandin E2 (PGE2) and NO, are increased when microglia are activated. They both have been identified as drug targets to dampen the inflammatory response and thus potentially impact the neurodegenerative processes (del Zoppo et al., 2000; Knott et al., 2000; Teismann et al., 2003; Yu et al., 2004; Mollace et al., 2005). In our hands, DCEFs had an effect on COX-2 expression, but not iNOS levels, in quiescent BV2 cells when using higher voltages (100V/m), which reflect the fact that the expression kinetic between these molecules may not always follow identical patterns. For example, in fibroblasts, LPS-induced COX-2 secretion was stable between 24 and 48 hours after LPS activation, while the production of iNOS peaked at 24 hours and decreased afterwards (Zhu et al., 2012). Furthermore, we did not observe changes in the concentration of extracellular cytokines in any of the conditions tested. As a whole, our results show that DCEFs can impact microglial cell morphology without significantly modulating their responses, at least not under the conditions that we tested. Observations of DCEF effects on microglial cells have not been reported previously (Table 3).

However, several pathologies for which DCEFs could be used are characterized by a significant neuroinflammatory response, and our current knowledge of the type and magnitude of the neuroinflammatory reaction triggered or suppressed by DCEFs is very limited. In vitro evidence suggests that DCEFs can polarize and accelerate the migration of various types of peripheral immune cells, including lymphocytes (Li et al., 2011), monocytes (Lin et al., 2008) and neutrophils (Zhao et al., 2006), macrophages (Orida and Feldman, 1982), and polymorphonuclear cells (Franke and Gruler, 1990), but there has been no account of measurable functional changes. In rodents, high intensity (≥142.9 A/m^2) unilateral cathodal tDCS of the parietal cortex induces tissue damage (Liebetanz et al., 2009), whereas both unilateral cathodal and anodal tDCS of the motor cortex increases the number of microglia cells (ionized calcium-binding adapter molecule 1 (Iba1)$^{+}$) in stimulated structures (Rueger et al., 2012). At lower intensity (33.4 A/m^2), bilateral anodal tDCS over the parietal cortex lowers hippocampal TNFα protein levels in a rat model of chronic stress-induced pain (Spezia Adachi et al., 2012). In mice stimulated with cathodal tDCS (55.0 A/m^2) following middle

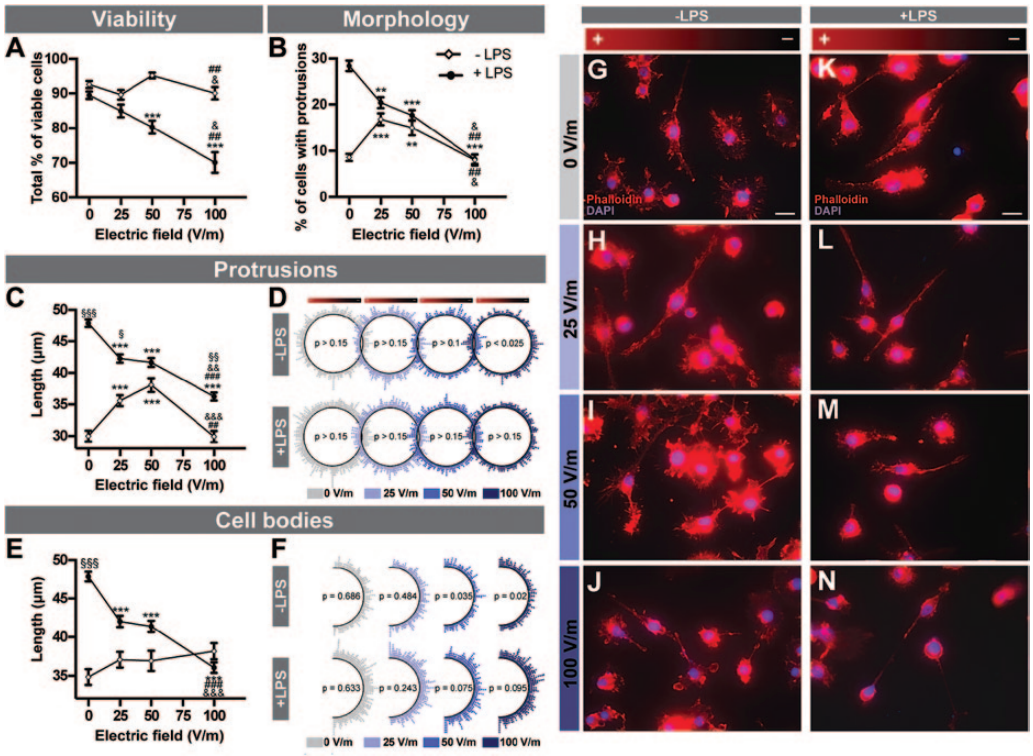

Figure 4. DCEF effects on microglial cells. (A) The viability of resting and LPS-activated BV2 mouse microglial cells (4–5 replicates, n total = 1350–2511) as well as (B) the total percentage of microglial cells specifically presenting protrusions (4–7 replicates, n total = 2314–2723) were both influenced by DCEFs. (C) The total length of protrusions in resting (4–5 replicates, n total = 423–670) and LPS-activated BV2 cells (6–7 replicates, n total = 522–877) was also affected by various DCEFs. (D) Polar distribution of protrusion angles (each dot represents the angle of a single protrusion). Quiescent BV2 cells reoriented parallel to the DCEF when exposed to 100V/m (6–7 replicates, n total = 522–877), but protrusion orientation was evenly distributed (i.e. did not show any specific directional preference) in LPS-activated BV2 cells in all conditions (4–5 replicates, n total = 423–670). (E) Total cell body length was similar in all conditions for resting microglia (4–5 replicates, n total = 437–593) but was significantly reduced following LPS treatment (6–7 replicates, n total = 263–371). (F) Polar distribution of the cell body angles (each dot represents the angle of a single cell body). Cell body orientation was similar in all DCEF intensities for LPS-activated BV2 cells but was parallel to the DCEF at 50 and 100V/m for resting BV2 cells (6–7 replicates, n total = 263–371). (G-N) Photomicrographs of double phalloidin (F-actin, red) and DAPI (nucleus, blue) immunofluorescent staining showing the morphological and orientational changes in BV2 microglial cells in response to DCEFs. Scale bar: 20 µm. (A-B, C, E) Data are presented as LS-means ± SEM. Statistical analyses: (A-B) ANOVA (split-plot-type, binomial), (C, E) ANOVA (split-plot-type) following log transformation, (D) Kuiper's Test of Uniformity, and (F) chi-square test using grouped data (number of classes = 8 with identical divisions for interval 0 to 180°). $^{**}P < .01$, $^{***}P < .001$ vs 0V/m; $^{\#\#}P < .01$, $^{\#\#\#}P < .001$ vs 25V/m; $^{\&}P < .05$, $^{\&\&}P < .01$, $^{\&\&\&}P < .001$ vs 50V/m; $\infty\infty P < .01$, $\infty\infty\infty P < .001$ vs resting cells (-LPS). DCEF, direct current electrical field; LPS, lipopolysaccharide; LS, least square; V/m, Volt/meter.

cerebral artery occlusion, Iba1$^+$ and CD45$^+$ cells are reduced in the ischemic cortex hours following stimulation of the damaged area (Peruzzotti-Jametti et al., 2013). These data support the concept that DCEF can have an effect on the behavior of microglial cells. Whether this response results from stimulation parameters or complex cell interactions, or both, will require further investigation.

Not surprisingly, astrocytes also react to DCEFs. It is known that DCEFs can align astrocytes perpendicular to the EF both in vitro (Borgens et al., 1994; Alexander et al., 2006) and in vivo (Moriarty and Borgens, 2001). In addition to confirming this effect in vitro, we demonstrated that protrusions and cell body length are affected by DCEFs and that they both reorient in a similar manner (Table 3). Previous studies have suggested that neurites realign according to the astrocyte position. In other words, the direction adopted by astrocytes dictates the direction of the growing neurites (Alexander et al., 2006). Despite these preliminary observations, the role of astrocytes in DCEF therapy is largely unknown. Interestingly, recent work on DBS argues that the induction of a significant astrocytic response actually enhances its effects (Fenoy et al., 2014), with the suggestion that the inevitable stimulation of astrocytes by DBS can set in motion the release of gliotransmitters that can in turn trigger axonal activation, which mediates part of the therapeutic benefits observed. Astrocytes, which can interact with more than 2 million synapses in the human brain, can thereby have a profound effect on synaptic activity across large neural networks (Oberheim et al., 2006; Cicchetti and Barker, 2014), and something similar may happen with tDCS. The complexity of cellular interactions and their impact on the observations we have made is certainly not fully accounted for in the in vitro setting. Future work using co-culture systems would be a first step in attempting to understand the impact of one cell response to DECF on another.

The approach of tDCS is currently the most common therapy to use DCEF, although its mechanisms of action are still poorly understood (for review, see Pelletier and Cicchetti, 2014). In vitro and in vivo animal studies conducted thus far are rare, and the parameters used (duration and intensity of stimulation) are so diverse from one study to the other that it is hard to interpret the data in the clinical setting. The DCEF parameters (25–100V/m) chosen for our study are very similar to the bulk of studies published in vitro and in vivo (Bikson et al., 2004; Kabakov et al., 2012). These intensities are admittedly higher than what is typically used in human tDCS, where stimulation amounts to ≤1V/m, for a maximum of 0.28 A/m^2 brain current

Table 1. Summary of Statistical Correlations

Figure	Cell type	Measure	Regression analysis	*P* Value	R^2
2D	N2a	Neurite length	Linear	P = .010	0.286
2F	N2a	Cell body length	Second-order polynomial	P = .011	0.376
4A	BV2 + LPS	Survival	Linear	P < .001	0.572
4B	BV2 + LPS	Percentage of cells with protrusions	Linear	P < .001	0.460
4C	BV2 - LPS	Protrusion length	Second order polynomial	P < .001	0.706
4C	BV2 + LPS	Protrusion length	Linear	P < .001	0.489
6C	C8-D1A	Protrusion length	Linear	P = .008	0.350
6E	C8-D1A	Cell body length	Linear	P < .001	0.712

Table 2. Cytokine Quantification

		0V/m			25V/m			50V/m			100V/m			ANOVA *P*
Cytokine	LPS	Mean	SD	N	Mean	SD	N	Mean	SD	N	Mean	SD	N	value
IL1α	+	3798	1157	8	2955	1197	7	4161	1244	6	4063	1194	7	.088
	-	2894	1636	4	3455	1636	4	2584	1754	3	1519	1636	4	.099
IL1β	+	634	127	8	510	132	7	556	138	6	535	131	7	.318
	-	336	179	4	339	179	4	521	194	3	329	179	4	.675
IL2	+	60	11	8	33	11	7	28	12	6	31	11	7	.071
	-	16	15	4	17	15	4	14	17	3	35	15	4	.360
IL3	+	101	19	8	72	20	7	73	21	6	83	20	7	.607
	-	58	27	4	82	27	4	74	29	3	55	27	4	.328
IL4	+	148	35	8	114	37	7	165	39	6	174	37	7	.416
	-	129	50	4	143	50	4	122	55	3	113	50	4	.785
IL5	+	775	164	8	527	174	7	514	186	6	823	174	7	.077
	-	455	232	4	642	232	4	568	263	3	615	232	4	.756
IL6	+	3294	672	8	1683	682	7	1659	695	6	1893	681	7	.055
	-	827	888	4	1186	888	4	464	913	3	556	888	4	.535
IL10	+	72	13	8	46	14	7	60	15	6	77	14	7	.127
	-	47	19	4	57	19	4	34	20	3	30	19	4	.170
IL12	+	2573	482	8	1841	508	7	1657	539	6	2287	507	7	.128
	-	1879	682	4	1953	682	4	2122	761	3	3187	682	4	.432
IL17	+	1842	306	8	1773	317	7	1546	330	6	2119	316	7	.122
	-	2062	433	4	2032	433	4	2258	465	3	1984	433	4	.946
GMCSF	+	645	163	8	634	167	7	667	171	6	594	166	7	.995
	-	542	231	4	411	231	4	729	241	3	796	231	4	.130
TNFα	+	2732	625	8	1904	649	7	1841	678	6	2143	648	7	.073
	-	2560	884	4	2508	884	4	2175	956	3	3469	884	4	.860
RANTES	+	17593	10146	8	14353	10548	7	37310	11026	6	13310	10520	7	.054
	-	3883	14348	4	8520	14348	4	7145	15549	3	6507	14348	4	.854
IFNγ	+	520	161	8	407	167	7	380	173	6	512	166	7	.369
	-	399	228	4	358	228	4	333	244	3	810	228	4	.277

Abbreviations: GMCSF, granulocyte-macrophage colony-stimulating factor; IL, interleukin; IFNγ, interferon gamma; LPS, lipopolysaccharide; RANTES, regulated on activated, normal T cell expressed and secreted; SD, standard deviation; TNFα, tumor-necrosis factor alpha.

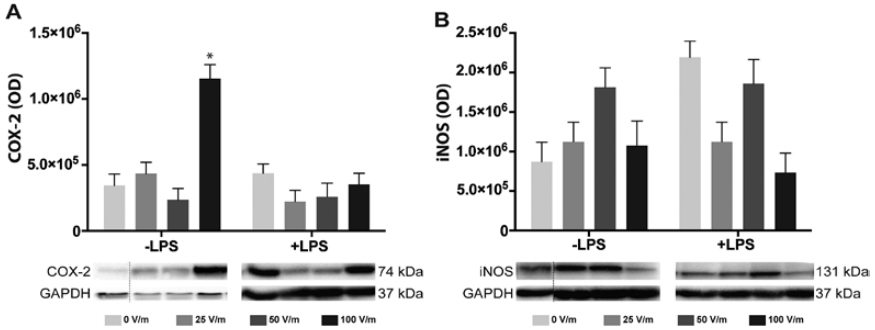

Figure 5. DCEF effects on inflammatory markers associated with microglial cells. The expression of COX-2 (A) and iNOS (B) was quantified by Western-blot analyses, but no significant changes were noted except for COX-2 expression in BV2 resting microglial cells exposed to 100V/m DCEF. The immunoblots are delineated by a dotted line when they originate from different parts of the same gel. Protein quantification and GAPDH staining determined the homogeneity of sample loading. Values represent LS-means ± SEM. Statistical analyses: split plot ANOVA following log transformation. *P < .05 compared with 0V/m in cells not exposed to LPS (-LPS). COX-2, cyclooxygenase-2; DCEF, direct current electrical field; GAPDH, glyceraldehyde 3-phosphate dehydrogenase; iNos, inducible nitric oxide synthase; LPS, lipopolysaccharide; OD, optical density.

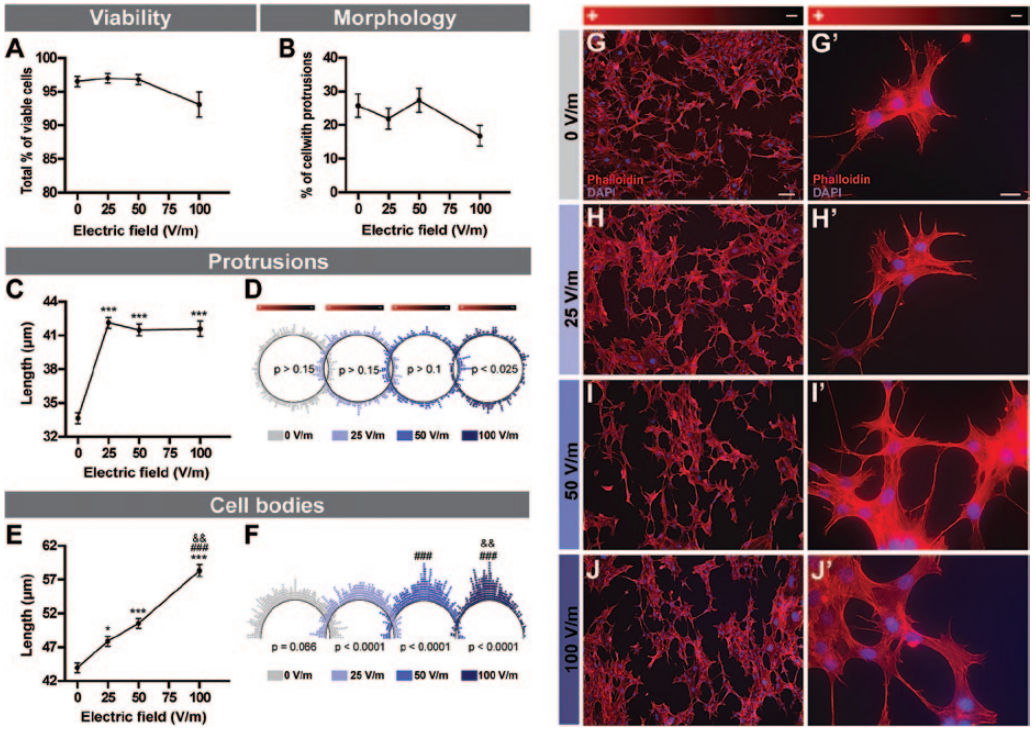

Figure 6. DCEF effects on astrocytes. (A) The viability of C8-D1A murine astrocytes (3–4 replicates, n total = 321–724) and (B) the total percentage of cells presenting protrusions (4–5 replicates, n total = 586–837) were similar across all DCEFs applied (from 0 to 100V/m). (C) The total length of protrusions (4–5 replicates, n total = 278–450) was increased following stimulation with 25, 50, and 100V/m. (D) Polar distribution of the protrusions (each dot represents the angle of a single protrusion). The cell protrusions were oriented perpendicularly (4–5 replicates, n total = 278–450) to the DCEF at 100V/m. (E) The total length of cell bodies (4–5 replicates, n total = 437–593) steadily increased in 25, 50, and 100V/m DCEF. (F) Polar distribution of cell body angles (each dot represents the angle of a single cell body). The cell bodies were oriented perpendicular (4–5 replicates, n total = 437–593) to the DCEF at 25, 50, and 100V/m. The homogeneity of cell body orientation was more prominent with increasing voltages. (G-J) Photomicrographs of double phalloidin (F-actin, red) and DAPI (nucleus, blue) immunofluorescent staining illustrating the morphological and orientational changes in C8-D1A mouse astrocytes in response to DCEFs. (Scale bars G-J: 100 µm, G'-J': 20 µm). (A-C, E) Data represents LS-means ± SEM. Statistical analyses: (A-B) ANOVA (split-plot-type, binomial), (C, E) ANOVA (split-plot-type) following log transformation. (D) Kuiper's Test of Uniformity (F) chi-square test using grouped data (number of classes = 8 with identical divisions for interval 0–180°). $^{*}P < 0.05$, $^{***}P < .001$ vs 0V/m; $^{\#\#\#}P < .001$ vs 25V/m; $^{\&\&}P < .01$ vs 50V/m. DCEF, direct current electrical field; LS, least square; V/m, Volt/meter.

Table 3. Responses of Cells of the CNS to DCEF

Cell types	Cell lines or primary cell	Electric field (V/m)	Length of exposure (h)	Main published observations/ novel observations	References
Neurons	Derived from dorsal root ganglia of chick embryos	15–140	3.7–6.3	• Neurites grow faster towards the cathode.	(Jaffe and Poo, 1979)
Neurons	Derived from neural tube of *Xenopus laevis* embryos	4–190	16–20	• 7V/m is identified as the minimal DCEF to induce a change in direction of neurites (towards the cathode). • More neurons grow neurites in 6–8V/m DCEF.	(Hinkle et al., 1981)
Neurons	Derived from neural tube of *Xenopus laevis* embryos	100–1000	6	• Neurite growth towards the cathode is accelerated, and decelerated towards the anode. • Those perpendicular to the field change direction towards the cathode. • Neurite sprouting is increased towards the cathode. • The total number of neurons with neurites, as well as neurite length, are increased. These effects are abolished by concanavalin A.	(Patel and Poo, 1982)

(*Continued*)

Table 3. *Continued*

Cell types	Cell lines or primary cell	Electric field (V/m)	Length of exposure (h)	Main published observations/ novel observations	References
Neurons	Derived from neural tube of *Xenopus laevis* embryos	50–155	3	• Reabsorption/retraction of neurites facing the anode. • Fewer filipodia on neurites facing the anode and more on neurites facing the cathode.	(McCaig, 1987)
Neurons	NlE-115 mouse neuroblastoma cells	100–1000	1	• Increase in sprouting, change of direction and growth rate in neurites facing the cathode. • Increase of reabsorption of neurites facing the anode. • Increase in extracellular calcium in the cell compartment facing the cathode.	(Bedlack et al., 1992)
Neurons	PC12 cells	5–100	48	• Increase in the total of number neurites oriented towards the anode.	(Cork et al., 1994)
Neurons	Derived from spinal neurons of *Xenopus laevis* embryos	50–200	4	• Branching and direction change in neurites towards the cathode are blocked by aminoglycosides (inositol phospholipid inhibitor). • Combined exposure to neomycin (polyphosphoinositide metabolism inhibitor) and extracellular Ca2+ reverses these effects. • Neurite growth rate is modified by aminoglycosides and external Ca2+.	(Erskine et al., 1995)
Neurons	Derived from neural tube of *Xenopus laevis* embryos	50–200	5	• Increased changes in direction, branching and growth rate towards the cathode are modulated by voltage-gated calcium channels and intracellular calcium storage.	(Stewart et al., 1995)
Neurons	Derived from neural tube of *Xenopus laevis* embryos	100	12	• Change in direction of neurites towards the cathode is independent of intracellular and extracellular Ca2+.	(Palmer et al., 2000)
Neurons	Derived from neural tube of *Xenopus laevis* embryos	50–200	5	• Neurotrophins promote growth cone guidance and neurite sprouting towards the cathode but decrease neurite growth towards the anode.	(McCaig et al., 2000)
Neurons	Derived from spinal neurons of *Xenopus laevis* embryos	150	5	• Dynamics of microfilaments and microtubules is essential for the migration of neurites towards the cathode.	(Rajnicek et al., 2006b)
Neurons	Derived from spinal neurons of *Xenopus laevis* embryos	150	5	• Rho, Rac and Cdc42 (of the Rho family of GTPases) are necessary for the initial neurite change in direction towards the cathode. • Following 2 h of stimulation, Rho and Cdc42 are still important but Rac signaling dominates. • PI-3K, MAPK and ERK1/2 are not needed for redirection towards the cathode.	(Rajnicek et al., 2006a)
Neurons	Derived from dorsal root ganglia of chick embryos	24–44	0.167–1.167	• Neurite length is greater 24 h after DCEF stimulation. • This is not influenced by the type of media, the surface coating nor growth supplements.	(Wood and Willits, 2009)

(*Continued*)

Table 3. *Continued*

Cell types	Cell lines or primary cell	Electric field (V/m)	Length of exposure (h)	Main published observations/ novel observations	References
Neurons	Rat dorsal root ganglion	10–100	8	• Neurite outgrowth is enhanced by DCEF. • This outgrowth is greater in co-cultures of neurons and Schwann cells.	(Koppes et al., 2011)
Neurons	N2a cells	25–100	24	• No differences in cell viability between stimulation intensities. • Cell bodies orient parallel to the DCEF and elongate when stimulated at 25 and 50V/m. • Neurites are elongated and reoriented towards the cathode. • GAP-43 protein is increased at 25 and 50V/m.	Present observations
Neurons	Dopaminergic explants	50	24	• Neurites orient and are longer towards the cathode.	Present observations
Astrocytes	Rat primary cortical asctrocytes	50–500	7–15.5	• Cell protrusions reorient perpendicularly the DCEF following an initial retraction of the neurites followed by an extension.	(Borgens et al., 1994)
Astrocytes	Rat primary cortical asctrocytes	50–1500	0.5	• Reduced glycolysis rate at 50V/m, unchanged at 100V/m and increased at >150V/m.	(Huang et al., 1997)
Astrocytes	Rat primary cortical asctrocytes	500	24	• Cells align perpendicularly to the electric field.	(Alexander et al., 2006)
Astrocytes	C8-D1A cells	25–100	24	• Cells bodies and protrusions are elongated. • Cells bodies and protrusions align perpendicularly to the electric field.	Present observations
Microglia	Quiescent BV-2 cells	25–100	24	• The number of cells with protrusions is increased at 25 and 50V/m. • Cell protrusion length is increased at 25V/m and 50V/m. • Cell bodies and protrusions reorient perpendicular to the electric field. • COX-2 expression is increased at 100V/m.	Present observations
Microglia	Activated BV-2 cells	25–100	24	• The number of viable cells and cells with protrusions is reduced by the electric field. • Shrinking of cell bodies and protrusions.	Present observations

Abbreviations: Cdc42, cell division control protein 42 homolog; COX-2, cyclooxygenase-2; DCEF, direct current electric field; ERK1/2, extracellular-signal-regulated kinase; GAP-43, growth-associated protein-43; GTP, guanosine triphosphate; PI-3K, phosphoinositide 3-kinase; MAPK, mitogen-activated protein kinase; Rac, ras-related C3 botulinum toxin substrate.

density (Minhas et al., 2012). In animal studies, brain current density has reached up to 142.0 A/m^2.

DCEF-induced cellular responses have been consistently demonstrated to be dependent on the length (Bedlack et al., 1992; Erskine et al., 1995; Zhao et al., 2004a; Rajnicek et al., 2006a 2006b) and intensity of the EF applied (Li and Kolega, 2002; Bai et al., 2004; Rajnicek et al., 2006a 2006b). It is thus likely that tDCS in humans, which is delivered over relatively short periods of time and at weaker intensities, leads to more subtle modulations than those reported in our study. However, the effects observed with tDCS could originate from an impact on the plasticity of existing synapses, as this response is much quicker than actual morphological changes. In vitro brain slices as well as animal and human experiments have all provided evidence that tDCS affects neurotransmitter release (for review, see Pelletier and Cicchetti, 2014). However, morphological changes induced by DCEFs have, thus far, been reported only in monolayer cultures or a guinea pig model of spinal cord injury (Borgens, 1999; Moriarty and Borgens, 2001). In this particular case, which used stimulation intensity lower than those used in human tDCS but for longer duration (Nitsche et al., 2008), both axon and astrocyte morphology demonstrated significant changes as observed in vitro. This not only supports the observations reported in our study as well as in other experiments using monolayer cultures

Table 4. Summary of Results

Cell Type	Viability		Cells with Protrusions (%)		Protrusion Length		Protrusion Orientation in EF		Cell Body Length		Cell body Orientation in EF		Molecular Responses	
N2a	–	All	–	All	↑	All	To cathode	All	↑	25–50 V/m	∥	All	↑	GAP-43	25–50 V/m
DA explants	NT		NT		↓	50 V/m	To cathode	50 V/m	NT		NT		NT		
BV2 -LPS	–	All	↑	25–50 V/m	↑	25–50 V/m	∥	100 V/m	–	All	∥	50–100 V/m	↑	COX-2	100 V/m
													–	iNOS	All
													–	Cytokines	All
BV2 +LPS	↓	50–100 V/m	↓	All	↓	All	–	All	↓	All	–	All	–	COX-2	All
													–	iNOS	All
													–	Cytokines	All
C8-D1A	–	All	–	All	↑	All	⊥	100 V/m	↑	All	⊥	All	–	GDNF	All

Abbreviations: ↓, reduced; ↑, increased; –, no response; All, all conditions; COX-2, cyclooxygenase-2; DA, dopamine; EF, electric field; GAP-43, growth-associated protein-43; GDNF, glial derived neurotrophic factor; iNOS, inducible nitric oxide synthase; LPS, lipopolysaccharide; NT, not tested; ⊥, perpendicular; ∥, parallel; V/m, Volt/meter.

(Patel and Poo, 1982; Borgens et al., 1994) but also suggests that similar changes could occur in human tDCS. Furthermore, the increase of GAP-43 and microtubule associated protein-2 (MAP-2) (Yoon et al., 2012) after 5 × 20-minute tDCS sessions (28.2 A/m^2) in rats provides evidence that axonal morphology can be modified using stimulation periods as short as those utilized in humans. The relevance of tDCS parameters used in animal experiments further finds support in the behavioral outcomes that have been reported to be similar in several animal models of disease (eg, improvements of motor features in Parkinson's disease patients and a rat model of the disease and anticonvulsive properties in epileptic patients as in a rat model of epilepsy). This has been extensively discussed in Pelletier and Cicchetti (2014).

This disparity between human, animal, and in vitro tDCS parameters does not necessarily invalidate the results obtained in animals nor in in vitro studies, as the latter setting offers a number of advantages over more complex systems. Electric current direction and intensity can easily be manipulated in in vitro models (Bikson et al., 2012), which may in turn facilitate the understanding of cellular and molecular mechanisms involved in this approach. Nevertheless, data interpretation in vitro should be made with caution and ultimately confirmed in vivo. Importantly, stimulation parameters in humans are still largely unexplored, and optimal conditions have yet to be identified. The tolerability and safety of higher current densities, which may be more desirable in acute disease contexts, remain to be tested (Nitsche et al., 2008).

Conclusion

Using an in-house DCEF prototype on 3 representative cell types of the central nervous system, our study provides evidence that cells respond to EFs, as shown by changes in their morphology, elongation, and retraction of their neurites/protrusions with some changes in their molecular responses. Despite the fact that tDCS is still at an early stage of clinical application, the in vitro and in vivo observations to date are encouraging and warrant further investigation. This will allow for a better understanding of how the therapy may work and, with this, the ability to better use it with greater effect in patients suffering from various brain disorders.

Acknowledgments

This work was supported by the Parkinson Society Canada to F.C., who is also the recipient of a National Researcher career award from the Fonds de recherche du Québec en santé (FRQS) proving salary support and operating funds. I.S.-A. was supported by a fellowship from a joint program of the Huntington Society of Canada and Canadian Institutes of Health Research and G.C. by a doctoral scholarship from Centre thématique de recherche en neurosciences of Université Laval. M.L. was supported by the Natural Sciences and Engineering Research Council of Canada; salary support was also provided by FRQS. The authors also thank Dr Meng Li for providing the *Pitx3-GFP* mice, Gilles Chabot for artwork, and Gaétan Daigle for statistical analyses.
Interest Statement: None.

References

Aigner L, Arber S, Kapfhammer JP, Laux T, Schneider C, Botteri F, Brenner HR, Caroni P (1995) Overexpression of the neural growth-associated protein GAP-43 induces nerve sprouting in the adult nervous system of transgenic mice. Cell 83:269–278.

Alais S, Simoes S, Baas D, Lehmann S, Raposo G, Darlix JL, Leblanc P (2008) Mouse neuroblastoma cells release prion infectivity associated with exosomal vesicles. Biol Cell 100:603–615.

Alexander JK, Fuss B, Colello RJ (2006) Electric field-induced astrocyte alignment directs neurite outgrowth. Neuron Glia Biol 2:93–103.

Alhouayek M, Muccioli GG (2014) COX-2-derived endocannabinoid metabolites as novel inflammatory mediators. Trends Pharmacol Sci 35:284–292.

Auvichayapat N, Rotenberg A, Gersner R, Ngodklang S, Tiamkao S, Tassaneeyakul W, Auvichayapat P (2013) Transcranial direct current stimulation for treatment of refractory childhood focal epilepsy. Brain Stimul 6:696–700.

Babona-Pilipos R, Droujinine IA, Popovic MR, Morshead CM (2011) Adult subependymal neural precursors, but not differentiated cells, undergo rapid cathodal migration in the presence of direct current electric fields. PLoS One 6:e23808.

Baetge EE, Hammang JP (1991) Neurite outgrowth in PC12 cells deficient in GAP-43. Neuron 6:21–30.

Bai H, McCaig CD, Forrester JV, Zhao M (2004) DC electric fields induce distinct preangiogenic responses in microvascular and macrovascular cells. Arterioscler Thromb Vasc Biol 24:1234–1239.

Bedlack RS Jr, Wei M, Loew LM (1992) Localized membrane depolarizations and localized calcium influx during electric field-guided neurite growth. Neuron 9:393–403.

Benninger DH, Lomarev M, Lopez G, Wassermann EM, Li X, Considine E, Hallett M (2010) Transcranial direct current stimulation for the treatment of Parkinson's disease. J Neurol Neurosurg Psychiatry 81:1105–1111.

Benowitz LI, Routtenberg A (1997) GAP-43: an intrinsic determinant of neuronal development and plasticity. Trends Neurosci 20:84–91.

Biewenga JE, Schrama LH, Gispen WH (1996) Presynaptic phosphoprotein B-50/GAP-43 in neuronal and synaptic plasticity. Acta Biochim Pol 43:327–338.

Biffo S, Verhaagen J, Schrama LH, Schotman P, Danho W, Margolis FL (1990) B-50/GAP43 expression correlates with process outgrowth in the embryonic mouse nervous system. Eur J Neurosci 2:487–499.

Bikson M, Inoue M, Akiyama H, Deans JK, Fox JE, Miyakawa H, Jefferys JG (2004) Effects of uniform extracellular DC electric fields on excitability in rat hippocampal slices in vitro. J Physiol 557:175–190.

Bikson M, Datta A, Elwassif M (2009) Establishing safety limits for transcranial direct current stimulation. Clin Neurophysiol 120:1033–1034.

Bikson M, Reato D, Rahman A (2012) Cellular and network effects of transcranial direct current stimulation: insights from animal models and brain slice. In: transcranial brain stimulation (Miniussi C, Paulus W, Rossini PM, eds), pp 55–92. Boca Raton, FL: CRC Press/Taylor & Francis.

Boggio PS, Ferrucci R, Rigonatti SP, Covre P, Nitsche M, Pascual-Leone A, Fregni F (2006) Effects of transcranial direct current stimulation on working memory in patients with Parkinson's disease. J Neurol Sci 249:31–38.

Booth R, Kim H (2012) Characterization of a microfluidic in vitro model of the blood-brain barrier (muBBB). Lab Chip 12:1784–1792.

Borgens RB (1999) Electrically mediated regeneration and guidance of adult mammalian spinal axons into polymeric channels. Neuroscience 91:251–264.

Borgens RB, Shi R, Mohr TJ, Jaeger CB (1994) Mammalian cortical astrocytes align themselves in a physiological voltage gradient. Exp Neurol 128:41–49.

Buffo A, Holtmaat AJ, Savio T, Verbeek JS, Oberdick J, Oestreicher AB, Gispen WH, Verhaagen J, Rossi F, Strata P (1997) Targeted overexpression of the neurite growth-associated protein B-50/GAP-43 in cerebellar Purkinje cells induces sprouting after axotomy but not axon regeneration into growth-permissive transplants. J Neurosci 17:8778–8791.

Cicchetti F, Barker RA (2014) The glial response to intracerebrally delivered therapies for neurodegenerative disorders: is this a critical issue? Front Pharmacol 5:139.

Cork RJ, McGinnis ME, Tsai J, Robinson KR (1994) The growth of PC12 neurites is biased towards the anode of an applied electrical field. J Neurobiol 25:1509–1516.

Dell'osso B, Dobrea C, Arici C, Benatti B, Ferrucci R, Vergari M, Priori A, Altamura AC (2013) Augmentative transcranial direct current stimulation (tDCS) in poor responder depressed patients: a follow-up study. CNS Spectr:1–8.

del Zoppo G, Ginis I, Hallenbeck JM, Iadecola C, Wang X, Feuerstein GZ (2000) Inflammation and stroke: putative role for cytokines, adhesion molecules and iNOS in brain response to ischemia. Brain Pathol 10:95–112.

Erskine L, Stewart R, McCaig CD (1995) Electric field-directed growth and branching of cultured frog nerves: effects of aminoglycosides and polycations. J Neurobiol 26:523–536.

Evangelopoulos ME, Weis J, Kruttgen A (2005) Signalling pathways leading to neuroblastoma differentiation after serum withdrawal: HDL blocks neuroblastoma differentiation by inhibition of EGFR. Oncogene 24:3309–3318.

Fenoy AJ, Goetz L, Chabardes S, Xia Y (2014) Deep brain stimulation: are astrocytes a key driver behind the scene? CNS Neurosci Ther 20:191–201.

Franke K, Gruler H (1990) Galvanotaxis of human granulocytes: electric field jump studies. Eur Biophys J 18:335–346.

Gil V, del Rio JA (2012) Analysis of axonal growth and cell migration in 3D hydrogel cultures of embryonic mouse CNS tissue. Nat Protoc 7:268–280.

Goslin K, Schreyer DJ, Skene JH, Banker G (1988) Development of neuronal polarity: GAP-43 distinguishes axonal from dendritic growth cones. Nature 336:672–674.

Henn A, Lund S, Hedtjarn M, Schrattenholz A, Porzgen P, Leist M (2009) The suitability of BV2 cells as alternative model system for primary microglia cultures or for animal experiments examining brain inflammation. ALTEX 26:83–94.

Hinkle L, McCaig CD, Robinson KR (1981) The direction of growth of differentiating neurones and myoblasts from frog embryos in an applied electric field. J Physiol 314:121–135.

Huang R, Peng L, Hertz L (1997) Effects of a low-voltage static electric field on energy metabolism in astrocytes. Bioelectromagnetics 18:77–80.

Jacobsson SO, Fowler CJ (2001) Characterization of palmitoylethanolamide transport in mouse Neuro-2a neuroblastoma and rat RBL-2H3 basophilic leukaemia cells: comparison with anandamide. Br J Pharmacol 132:1743–1754.

Jaffe LF, Poo MM (1979) Neurites grow faster towards the cathode than the anode in a steady field. J Exp Zool 209:115–128.

Jain S, Sharma A, Basu B (2013) Vertical electric field stimulated neural cell functionality on porous amorphous carbon electrodes. Biomaterials 34:9252–9263.

Jiang T, Xu RX, Zhang AW, Di W, Xiao ZJ, Miao JY, Luo N, Fang YN (2012) Effects of transcranial direct current stimulation on hemichannel pannexin-1 and neural plasticity in rat model of cerebral infarction. Neuroscience 226:421–426.

Joung Lee S, Chun MH (2013) Combination transcranial direct current stimulation and virtual reality therapy for upper extremity training in subacute stroke patients. Arch Phys Med Rehabil 95:431–438.

Kabakov AY, Muller PA, Pascual-Leone A, Jensen FE, Rotenberg A (2012) Contribution of axonal orientation to pathway-dependent modulation of excitatory transmission by direct

current stimulation in isolated rat hippocampus. J Neurophysiol 107:1881–1889.
Kamida T, Kong S, Eshima N, Abe T, Fujiki M, Kobayashi H (2011) Transcranial direct current stimulation decreases convulsions and spatial memory deficits following pilocarpine-induced status epilepticus in immature rats. Behav Brain Res 217:99–103.
Kim SJ, Kim BK, Ko YJ, Bang MS, Kim MH, Han TR (2010) Functional and histologic changes after repeated transcranial direct current stimulation in rat stroke model. J Korean Med Sci 25:1499–1505.
Knott C, Stern G, Wilkin GP (2000) Inflammatory regulators in Parkinson's disease: iNOS, lipocortin-1, and cyclooxygenases-1 and -2. Mol Cell Neurosci 16:724–739.
Koppes AN, Seggio AM, Thompson DM (2011) Neurite outgrowth is significantly increased by the simultaneous presentation of Schwann cells and moderate exogenous electric fields. J Neural Eng 8:046023.
Li J, Nandagopal S, Wu D, Romanuik SF, Paul K, Thomson DJ, Lin F (2011) Activated T lymphocytes migrate toward the cathode of DC electric fields in microfluidic devices. Lab Chip 11:1298–1304.
Li X, Kolega J (2002) Effects of direct current electric fields on cell migration and actin filament distribution in bovine vascular endothelial cells. J Vasc Res 39:391–404.
Liebetanz D, Koch R, Mayenfels S, Konig F, Paulus W, Nitsche MA (2009) Safety limits of cathodal transcranial direct current stimulation in rats. Clin Neurophysiol 120:1161–1167.
Lin F, Baldessari F, Gyenge CC, Sato T, Chambers RD, Santiago JG, Butcher EC (2008) Lymphocyte electrotaxis in vitro and in vivo. J Immunol 181:2465–2471.
McCaig CD (1987) Spinal neurite reabsorption and regrowth in vitro depend on the polarity of an applied electric field. Development 100:31–41.
McCaig CD, Sangster L, Stewart R (2000) Neurotrophins enhance electric field-directed growth cone guidance and directed nerve branching. Dev Dyn 217:299–308.
McCaig CD, Rajnicek AM, Song B, Zhao M (2005) Controlling cell behavior electrically: current views and future potential. Physiol Rev 85:943–978.
Meiri KF, Pfenninger KH, Willard MB (1986) Growth-associated protein, GAP-43, a polypeptide that is induced when neurons extend axons, is a component of growth cones and corresponds to pp46, a major polypeptide of a subcellular fraction enriched in growth cones. Proc Natl Acad Sci U S A 83:3537–3541.
Michaud JP, Halle M, Lampron A, Theriault P, Prefontaine P, Filali M, Tribout-Jover P, Lanteigne AM, Jodoin R, Cluff C, Brichard V, Palmantier R, Pilorget A, Larocque D, Rivest S (2013) Toll-like receptor 4 stimulation with the detoxified ligand monophosphoryl lipid A improves Alzheimer's disease-related pathology. Proc Natl Acad Sci U S A 110:1941–1946.
Minhas P, Bikson M, Woods AJ, Rosen AR, Kessler SK (2012) Transcranial direct current stimulation in pediatric brain: a computational modeling study. Conf Proc IEEE Eng Med Biol Soc 2012:859–862.
Mollace V, Muscoli C, Masini E, Cuzzocrea S, Salvemini D (2005) Modulation of prostaglandin biosynthesis by nitric oxide and nitric oxide donors. Pharmacol Rev 57:217–252.
Moriarty LJ, Borgens RB (2001) An oscillating extracellular voltage gradient reduces the density and influences the orientation of astrocytes in injured mammalian spinal cord. J Neurocytol 30:45–57.
Nitsche MA, Cohen LG, Wassermann EM, Priori A, Lang N, Antal A, Paulus W, Hummel F, Boggio PS, Fregni F, Pascual-Leone A (2008) Transcranial direct current stimulation: state of the art 2008. Brain Stimul 1:206–223.
Oberheim NA, Wang X, Goldman S, Nedergaard M (2006) Astrocytic complexity distinguishes the human brain. Trends Neurosci 29:547–553.
Orida N, Feldman JD (1982) Directional protrusive pseudopodial activity and motility in macrophages induced by extracellular electric fields. Cell Motil 2:243–255.
Palmer AM, Messerli MA, Robinson KR (2000) Neuronal galvanotropism is independent of external Ca(2+) entry or internal Ca(2+) gradients. J Neurobiol 45:30–38.
Patel N, Poo MM (1982) Orientation of neurite growth by extracellular electric fields. J Neurosci 2:483–496.
Pelletier SJ, Cicchetti F (2014) Cellular and molecular mechanisms of action of transcranial direct current stimulation: evidence from in vitro and in vivo models. Int J Neuropsychopharmacol. doi:10.1093/ijnp/pyu047.
Pereira JB, Junque C, Bartres-Faz D, Marti MJ, Sala-Llonch R, Compta Y, Falcon C, Vendrell P, Pascual-Leone A, Valls-Sole J, Tolosa E (2013) Modulation of verbal fluency networks by transcranial direct current stimulation (tDCS) in Parkinson's disease. Brain Stimul 6:16–24.
Peruzzotti-Jametti L, Cambiaghi M, Bacigaluppi M, Gallizioli M, Gaude E, Mari S, Sandrone S, Cursi M, Teneud L, Comi G, Musco G, Martino G, Leocani L (2013) Safety and efficacy of transcranial direct current stimulation in acute experimental ischemic stroke. Stroke 44:3166–3174.
Rajnicek AM, Foubister LE, McCaig CD (2006a) Temporally and spatially coordinated roles for Rho, Rac, Cdc42 and their effectors in growth cone guidance by a physiological electric field. J Cell Sci 119:1723–1735.
Rajnicek AM, Foubister LE, McCaig CD (2006b) Growth cone steering by a physiological electric field requires dynamic microtubules, microfilaments and Rac-mediated filopodial asymmetry. J Cell Sci 119:1736–1745.
Rueger MA, Keuters MH, Walberer M, Braun R, Klein R, Sparing R, Fink GR, Graf R, Schroeter M (2012) Multi-session transcranial direct current stimulation (tDCS) elicits inflammatory and regenerative processes in the rat brain. PLoS One 7:e43776.
Shapiro S, Borgens R, Pascuzzi R, Roos K, Groff M, Purvines S, Rodgers RB, Hagy S, Nelson P (2005) Oscillating field stimulation for complete spinal cord injury in humans: a phase 1 trial. J Neurosurg Spine 2:3–10.
Sheng W, Zong Y, Mohammad A, Ajit D, Cui J, Han D, Hamilton JL, Simonyi A, Sun AY, Gu Z, Hong JS, Weisman GA, Sun GY (2011) Pro-inflammatory cytokines and lipopolysaccharide induce changes in cell morphology, and upregulation of ERK1/2, iNOS and sPLA(2)-IIA expression in astrocytes and microglia. J Neuroinflammation 8:121.
Song B, Gu Y, Pu J, Reid B, Zhao Z, Zhao M (2007) Application of direct current electric fields to cells and tissues in vitro and modulation of wound electric field in vivo. Nat Protoc 2:1479–1489.
Spezia Adachi LN, Caumo W, Laste G, Fernandes Medeiros L, Ripoll Rozisky J, de Souza A, Fregni F, Torres IL (2012) Reversal of chronic stress-induced pain by transcranial direct current stimulation (tDCS) in an animal model. Brain Res 1489:17–26.
Stewart R, Erskine L, McCaig CD (1995) Calcium channel subtypes and intracellular calcium stores modulate electric field-stimulated and -oriented nerve growth. Dev Biol 171:340–351.
Teismann P, Tieu K, Cohen O, Choi DK, Wu DC, Marks D, Vila M, Jackson-Lewis V, Przedborski S (2003) Pathogenic role of glial cells in Parkinson's disease. Mov Disord 18:121–129.
Vejlstrup NG, Bouloumie A, Boesgaard S, Andersen CB, Nielsen-Kudsk JE, Mortensen SA, Kent JD, Harrison DG, Busse R, Alder-

shvile J (1998) Inducible nitric oxide synthase (iNOS) in the human heart: expression and localization in congestive heart failure. J Mol Cell Cardiol 30:1215–1223.

Wang X, Zhang S, Sun C, Yuan ZG, Wu X, Wang D, Ding Z, Hu R (2011) Proteomic profiles of mouse neuro N2a cells infected with variant virulence of rabies viruses. J Microbiol Biotechnol 21:366–373.

Wood MD, Willits RK (2009) Applied electric field enhances DRG neurite growth: influence of stimulation media, surface coating and growth supplements. J Neural Eng 6:046003.

Yoon KJ, Oh BM, Kim DY (2012) Functional improvement and neuroplastic effects of anodal transcranial direct current stimulation (tDCS) delivered 1 day vs. 1 week after cerebral ischemia in rats. Brain Res 1452:61–72.

Yu Y, Matsuyama Y, Nakashima S, Yanase M, Kiuchi K, Ishiguro N (2004) Effects of MPSS and a potent iNOS inhibitor on traumatic spinal cord injury. Neuroreport 15:2103–2107.

Zhao M, Bai H, Wang E, Forrester JV, McCaig CD (2004a) Electrical stimulation directly induces pre-angiogenic responses in vascular endothelial cells by signaling through VEGF receptors. J Cell Sci 117:397–405.

Zhao M, Song B, Pu J, Wada T, Reid B, Tai G, Wang F, Guo A, Walczysko P, Gu Y, Sasaki T, Suzuki A, Forrester JV, Bourne HR, Devreotes PN, McCaig CD, Penninger JM (2006) Electrical signals control wound healing through phosphatidylinositol-3-OH kinase-gamma and PTEN. Nature 442:457–460.

Zhao S, Maxwell S, Jimenez-Beristain A, Vives J, Kuehner E, Zhao J, O'Brien C, de Felipe C, Semina E, Li M (2004b) Generation of embryonic stem cells and transgenic mice expressing green fluorescence protein in midbrain dopaminergic neurons. Eur J Neurosci 19:1133–1140.

Zhu Y, Zhu M, Lance P (2012) iNOS signaling interacts with COX-2 pathway in colonic fibroblasts. Exp Cell Res 318:2116–2127.